The Astrophysical Journal, 780:48 (10pp), 2014 January 1 doi:10.1088/0004-637X/780/1/48

MULTIWAVELENGTH OBSERVATIONS OF Swift J1753.5−0127

Cynthia S. Froning[1,7,8], Thomas J. Maccarone[2], Kevin France[1], Lisa Winter[3], Edward L. Robinson[4], Robert I. Hynes[5], and Fraser Lewis[6]
[1] Center for Astrophysics and Space Astronomy, University of Colorado, 593 UCB, Boulder, CO 80309-0593, USA; cynthia.froning@colorado.edu, kevin.france@colorado.edu
[2] Department of Physics, Texas Tech University, Box 41051, Lubbock, TX 79409, USA; t.j.maccarone@soton.ac.uk
[3] Space Weather and Effects Division, Atmospheric and Environmental Research, Superior, CO, USA; lwinter@aer.com
[4] Department of Astronomy, University of Texas at Austin, Austin, TX 78712, USA; elr@astro.as.utexas.edu
[5] Department of Physics and Astronomy, Louisiana State University, Baton Rouge, LA 70803, USA; rih@phys.lsu.edu
[6] Faulkes Telescope Project, University of South Wales, Astrophysics Research Institute, Liverpool John Moores University, UK; flewis@glam.ac.uk
Received 2013 August 30; accepted 2013 November 4; published 2013 December 11

ABSTRACT

We present contemporaneous X-ray, ultraviolet (UV), optical, and near-infrared observations of the black hole binary system Swift J1753.5−0127 acquired in 2012 October. The UV observations, obtained with the Cosmic Origins Spectrograph on the *Hubble Space Telescope*, are the first UV spectra of this system. The dereddened UV spectrum is characterized by a smooth, blue continuum and broad emission lines of C IV and He II. The system was stable in the UV to <10% during our observations. We estimated the interstellar reddening by fitting the 2175 Å absorption feature and fit the interstellar absorption profile of Lyα to directly measure the neutral hydrogen column density along the line of sight. By comparing the UV continuum flux to steady-state thin accretion disk models, we determined upper limits on the distance to the system as a function of black hole mass. The continuum is well fit with disk models dominated by viscous heating rather than irradiation. The broadband spectral energy distribution shows the system has declined at all wavelengths since previous broadband observations in 2005 and 2007. If we assume that the UV emission is dominated by the accretion disk, the inner radius of the disk must be truncated at radii above the innermost stable circular orbit to be consistent with the X-ray flux, requiring significant mass loss from outflows and/or energy loss via advection into the black hole to maintain energy balance.

Key words: accretion, accretion disks – binaries: close – stars: black holes – stars: individual (Swift J1753.5−0127)

Online-only material: color figures

1. INTRODUCTION

X-ray binaries (XRBs) are interacting binary systems in which a black hole or neutron star accretes material from a donor star, typically via an accretion disk. XRBs can occupy several different accretion states defined by their X-ray activity (McClintock & Remillard 2006). Systems in the low state have luminosities at or below several percent of their Eddington luminosities, although due to hysteresis effects in the transitions between states, there is not a strict monotonic relationship between luminosity and spectral state (Maccarone 2003; Maccarone & Coppi 2003). The low (or "low/hard") state systems are also characterized by hard, non-thermal X-ray spectra fit with power-law components with photon indices ∼1.7. This is generally ascribed to thermal Comptonization in a hot, optically thin corona located near the black hole or neutron star (Thorne & Price 1975; Shapiro et al. 1976; Sunyaev & Truemper 1979), though the source and physical properties of the corona are controversial. In contrast, XRBs in the high (or "high/soft") state have higher luminosities and a strong thermal component to the soft X-ray spectrum. The thermal component is interpreted as originating in the accretion disk and is fit by models of multi-temperature emission from a steady-state, thin disk, the temperature of which varies radially as $T(R) \propto R^{-3/4}$ (Shakura & Sunyaev 1973). XRBs in the low state are also host to persistent collimated outflows. Flat or inverted spectra have been observed in the radio to infrared regime in most XRBs in the low state, similar to the signature emission of jet cores in active galactic nuclei (Jain et al. 2001; Fender 2006; Russell et al. 2006). The spectra are attributed to self-absorbed synchrotron emission from a compact, highly collimated outflow that is quenched when a system transitions from the low to the high state (Tananbaum et al. 1972; Fender et al. 1999).

While great progress has been made in observing and modeling the behavior of XRBs, a number of questions remain unresolved, including the physical structure of the accretion disk, the link between accretion and outflows (in the forms of jets and winds), and the relative contributions of these components to the broadband spectral energy distributions (SEDs). Esin et al. (1997) presented a unified model of the accretion states of XRBs within the paradigm of advection-dominated accretion flows (ADAFs). In the ADAF model picture, a thin accretion disk in the low state is disrupted outside the innermost stable circular orbit (ISCO) of the black hole, forming a spherical, radiatively inefficient corona (Narayan & Yi 1995). Due to this radiatively inefficient corona, most of the accretion energy released by viscous dissipation is advected with the flow into the black hole. As a system transitions to the high state in outburst, the ADAF disappears and the thin disk extends to the ISCO. However, other models of the source of the X-ray corona in the low state have been advanced, including coronae driven by magnetic flares from the underlying accretion disk or emission from the base of the jet itself (Haardt & Maraschi 1991; Merloni & Fabian 2001a, 2001b; Markoff et al. 2001).

Multiwavelength observations provide powerful tools for studying the structure of the disks and outflows in XRBs. The

[7] Department of Astrophysical and Planetary Sciences, University of Colorado.
[8] University Affiliate Research Fellow, Department of Astronomy, University of Texas at Austin.

ultraviolet (UV) is a key component of these observations. UV continuum data probe the expected peak temperatures of thermal emission components in quiescent disks, while UV line emission traces the kinematics and abundances of accretion disk chromospheres (e.g., Froning et al. 2011; Bayless et al. 2010; Hynes et al. 2009; Haswell et al. 2002; McClintock & Remillard 2000). The UV can also directly test competing models of the structure of XRBs in the low state. In 2010, we obtained far-ultraviolet (FUV) observations of the black hole XRB, A0620−00 (Froning et al. 2011). The FUV component of the SED proved to be key to constraining accretion disk and jet models. Contrary to previous observations, the optical–UV spectrum did not continue to drop to shorter wavelengths, but instead showed a recovery and an increasingly blue spectrum in the FUV. The blue FUV trend, combined with the strong UV variability between observing epochs, was inconsistent with the previous ADAF model for A0620−00 (Narayan et al. 1997) and may indicate significant changes in the size of the ADAF and the thin disk/ADAF transition radius over time. Alternately, a comparison of the SED with a jet-dominated model showed good agreement and predicted that the increasing FUV flux originates in emission from the pre-acceleration inner jet component of the outflow.

In this manuscript, we continue our investigation of the FUV properties of XRBs and present the first FUV observations of Swift J1753.5−0127, obtained using the Cosmic Origins Spectrograph (COS) aboard the *Hubble Space Telescope* (*HST*; Green et al. 2012). Swift J1753.5−0127 is an X-ray transient discovered by the *Swift* Burst Alert Telescope when it went into outburst in 2005 (Palmer et al. 2005). It was soon detected in the UV, optical, near-infrared, and radio bands as well (Still et al. 2005; Halpern 2005; Torres et al. 2005; Fender et al. 2005). The shape of the hard X-ray spectrum was consistent with those of black hole XRBs in the hard state (Cadolle Bel et al. 2005). During its outburst, Swift J1753.5−0127 remained in the low state rather than transitioning to the high state, a behavior seen in other low-luminosity XRBs, including XTE J1118+480 and Swift J1357.2−0933 (Brocksopp et al. 2004; Hynes et al. 2000; Armas Padilla et al. 2013).

The system has not returned to quiescence since its 2005 outburst, and it remains active at X-ray and optical/infrared wavelengths (e.g., Shaw et al. 2013). Numerous fits to the X-ray spectrum of Swift J1753.5−0127 have differed in their conclusions concerning whether a thermal accretion disk component is present in the spectrum and whether the inner disk radius is located at the ISCO or at a larger radius (Miller et al. 2006; Ramadevi & Seetha 2007; Reis et al. 2009; Hiemstra et al. 2009; Reynolds et al. 2010; Mostafa et al. 2013). Here, we examine the broadband SED of Swift J1753.5−0127 7 yr after its initial outburst using COS observations combined with X-ray, optical, and near-infrared data obtained on the same day. In Section 2, we present the multiwavelength observations and data reduction. Section 3 shows the analysis of the UV spectrum and the SED. In Sections 4 and 5, we discuss the results and the conclusions from our work.

2. OBSERVATIONS AND DATA REDUCTION

On 2012 October 2 we obtained X-ray, UV, optical, and near-infrared (NIR) observations of Swift J1753.5−0127. The observations are summarized in Table 1. The X-ray and UV observations were simultaneous, while the optical/NIR data were acquired several hours earlier.

Table 1
Observation Summary

Telescope	Instrument	Grating/Filter	Date (UT)	Time (UT)	T_{exp} (s)
APO	SPIcam	*BVRI*	2012 Oct 2	01:40	360–700
APO	NIC-FPS	*JHK*	2012 Oct 2	02:59	108–180
HST	COS	G130M	2012 Oct 2	08:14	5126
HST	COS	G160M	2012 Oct 2	11:24	5683
HST	COS	G230L	2012 Oct 2	14:34	2839
SWIFT	XRT	···	2012 Oct 2	08:35	2120
SWIFT	UVOT	*U*	2012 Oct 2	08:39	2112

2.1. HST UV Spectroscopy

We observed Swift J1753.5−0127 with COS on 2012 October 2. Information about the design and on-orbit performance of COS can be found in Osterman et al. (2011), Green et al. (2012), and in the COS Instrument Handbook (Holland et al. 2012). We used the G130M and G160M gratings to obtain the FUV (1150–1800 Å) spectrum at moderate spectral resolution ($R \simeq 18{,}000$). We stepped each grating through four central wavelength positions to minimize the effects of fixed pattern noise. We also obtained NUV spectra using the G230L grating taken in two grating tilt positions (the 2950 Å and 3360 Å settings). Each G230L exposure covers three non-contiguous spectral regions, so the two tilt positions together subtend 1650–3560 Å with some gaps. The spectral resolution of the G230L data is $R \simeq 3000$.

We retrieved the COS data from the Multi-Mission Archive at STScI (MAST). The data had been processed with V. 2.18.5 of CALCOS. For the FUV data, we coadded the output one-dimensional spectral data products using a custom IDL code described in Danforth et al. (2010).[9] The code combines different wavelength settings and creates a weighted mean spectrum (with lower weight given to regions of uncertain flux calibration near detector edges). For the NUV spectra, we used the X1D files as delivered by CALCOS.

2.2. Swift X-Ray and UV Imaging

Swift acquired pointed observations of Swift J1753.5−0127 for 2100 s on 2012 October 2, simultaneous with the *HST*/COS observations. We retrieved and calibrated the X-Ray Telescope (XRT; Burrows et al. 2005) and UV/Optical Telescope (UVOT; Roming et al. 2005) data. The XRT was in windowed timing mode for the observation. A total of 12,355 X-ray counts were detected. The background is ≃20 photons, so a background subtraction in the spectrum was neglected during the analysis. For the UVOT data, we used the Swift FTOOL[10] uvotsource to extract the background-subtracted flux from the UVOT observations in the *U* filter. The *U*-band magnitude is given in Table 2.

For the XRT observation, we fit the data with an absorbed power-law model (phabs*powerlaw in XSPEC version 12.0; Arnaud 1996). If the foreground absorption is allowed to float freely, we find $N_{\rm H} = 2.66 \pm 0.14 \times 10^{21}\,{\rm cm}^{-2}$ and $\Gamma = 2.00 \pm 0.04$, with the errors assumed to be purely statistical and the uncertainties given at the 90% confidence level. The fit has $\chi^2_\nu = 1.01$ (with 769 dof). The absorbed flux in the 0.3–8 keV band is 2.37×10^{-10} erg cm^{-2} s^{-1}, and the unabsorbed flux in the same band is 3.8×10^{-10} erg cm^{-2} s^{-1}. If we fix the interstellar

[9] See also http://casa.colorado.edu/~danforth/science/cos/costools.html.
[10] See http://heasarc.gsfc.nasa.gov/docs/software/ftools/ftools_menu.html.

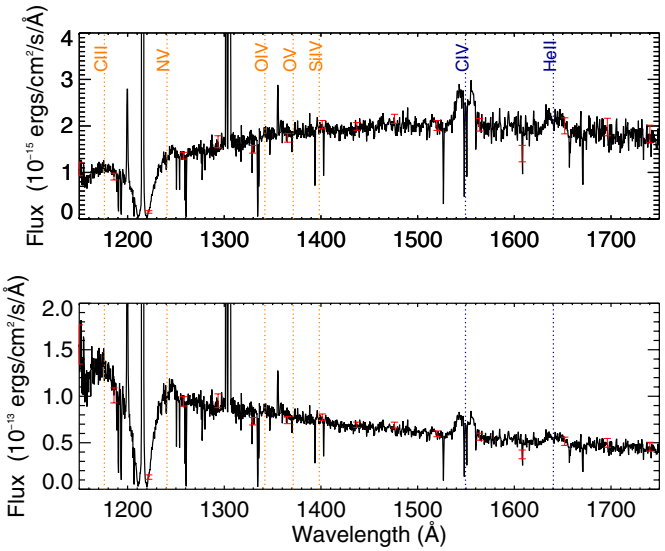

Figure 1. Time-averaged COS FUV spectrum of Swift J1753.5−0127. The data have been binned to six resolution elements (≃0.36 Å) and typical statistical error bars on the binned data are shown in red. The upper panel shows the observed spectrum while the lower panel shows the spectrum after it has been dereddened assuming $E(B-V) = 0.45$. Prominent emission lines detected in the spectrum are labeled in blue. Emission lines often observed in the FUV spectra of other X-ray binaries but not detected unambiguously in Swift J1753.5−0127 are labeled in orange. The narrow emission features at 1200 Å, 1215 Å 1304 Å, and 1356 Å are due to terrestrial airglow and the absorption lines are interstellar.

(A color version of this figure is available in the online journal.)

Table 2
Optical and NIR Photometry

Filter	Magnitude
U	16.19 ± 0.02[a]
B	17.143 ± 0.007
V	16.886 ± 0.004
R	16.581 ± 0.003
I	16.166 ± 0.003
J	15.55 ± 0.02
H	15.18 ± 0.03
K	14.89 ± 0.05

Note. [a] *Swift* uvotsource magnitude calibrated in the Vega system.

hydrogen absorption at the value found by our fits to the Lyα absorption line profile ($N_{\rm H} = 2.0 \times 10^{21}$ cm^{-2}; see Section 3.2), we obtain $\Gamma = 1.81 \pm 0.02$ and $\chi^2_\nu = 1.11$ (768 dof). The 0.3–8.0 keV unabsorbed flux is 2.45×10^{-10} erg cm^{-2} s^{-1} for this model. There was no significant improvement to the X-ray fits if we added additional components such as a thermal accretion disk component or a Gaussian emission component in the 6–7 keV range.

2.3. Apache Point Observatory Optical and Near-infrared Imaging

We obtained optical and NIR photometry of Swift J1753.5−0127 using SPIcam and NIC-FPS (Hearty et al. 2004) on the 3.5 m telescope at Apache Point Observatory, taking exposures in the B, V, R, I, J, H, and K filters. Weather conditions were clear with moderate, variable seeing (FWHM ≃ 0.″9–1.″5). We reduced the data using IRAF[11] for standard calibration tasks (e.g., bias subtraction, sky subtraction, and flat-fielding) and aperture photometry. We calibrated the photometry in the optical using the in-field standards given in Zurita et al. (2008). For the NIR, we acquired separate standards from the ARNICA catalog (Hunt et al. 1998). We averaged the results for multiple exposures for the target and standard star fields. The results are tabulated in Table 2. The uncertainties on the magnitudes are the propagated statistical errors for our exposures; because Swift J1753.5−0127 is variable, the observed magnitudes fluctuate at levels that are larger than the statistical errors.

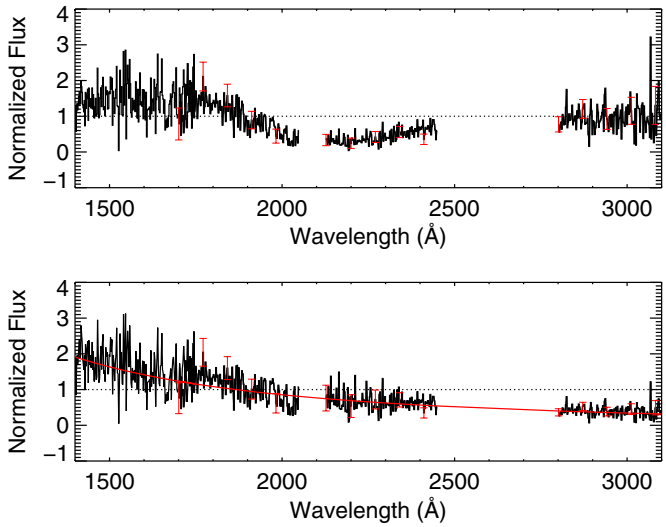

Figure 2. COS NUV spectrum in the vicinity of the 2175 Å interstellar absorption was fit to determine the reddening correction for the line of sight to Swift J1753.5−0127. The upper panel shows normalized G160M (from 1400–1750 Å) and G230L spectra (>1700 Å). The data have been binned to 1.6 Å resolution. The lower panel shows the spectrum after it has been dereddened using the best-fit value of $E(B-V) = 0.45$. The best fit was found by minimizing the χ^2 around a power-law fit to the dereddened spectrum, shown by the red line.

(A color version of this figure is available in the online journal.)

3. ANALYSIS

3.1. The Ultraviolet Spectrum

The FUV spectrum of Swift J1753.5−0127 is shown in Figure 1. The observed spectrum has a FUV continuum flux of 2×10^{-15} erg cm^{-2} s^{-1} Å^{-1} at 1450 Å. Spectral features include broad emission lines of C IV λλ1548,1551 and He II λ1640 and interstellar absorption features (Morton 1978). In Figure 1, we labeled the locations of other FUV lines that are often seen in the spectra of XRBs; however, only C IV and He II are clearly detected in Swift J1753.5−0127. There is an enhancement in the spectrum around 1240 Å that suggests the presence of the N V λλ1238,1242 doublet, but most of the line, if present, is lost in the broad interstellar Lyα absorption.

We dereddened the spectrum using $E(B-V) = 0.45$ (see Section 3.2). The dereddened spectrum shows a smooth continuum increasing to short wavelengths. The NUV spectrum extends the continuum to the red and shows no spectral features (see Figure 2). We fit single Gaussian profiles to the two

[11] IRAF is distributed by the National Optical Astronomy Observatory, which is operated by the Association of Universities for Research in Astronomy, Inc., under cooperative agreement with the National Science Foundation.

emission lines in the dereddened spectrum using Specfit (Kriss 1994). The fit to C IV also included coincident interstellar lines to correct for their effects on the line flux. The C IV and He II line fluxes are $5.5 \pm 0.8 \times 10^{-13}$ erg cm^{-2} s^{-1} and $2.6 \pm 0.6 \times 10^{-13}$ erg cm^{-2} s^{-1}, respectively. Both lines have FWHM $\simeq$ 3500 km s^{-1}; the widths are not constrained to better than approximately 500 km s^{-1}. We do not have the signal to noise to determine if the emission lines are single- or double-peaked. Using the observed flux density in the region of the N V doublet and correcting for the interstellar absorption, we set an upper limit on the N V line flux of $\lesssim 2.5 \times 10^{-14}$ erg cm^{-2} s^{-1}.

Using the COS time-tagged photon event list, we searched for variability in the continuum and emission lines during the observations. We identified regions of interest in the two-dimensional (wavelength versus cross-dispersion position) corrected time-tag spectral images and summed the counts in each image for selected time bins, subtracting a background region of the same size but offset from the target spectrum in the cross-dispersion direction for each bin. We selected several line-free continuum regions and the C IV and He II emission lines, examining the data in 50 s and 200 s time intervals. We used different grating tilt settings during the observation, so we restricted our analysis to the time intervals when our chosen wavebands were fully on the detector. We were insensitive to low-level variability because of the faintness of the target: we could not detect fluctuations (at $>3\sigma$) below 10% on 50 s time scales. Above that limit, the COS data were steady over the course of the observations. There were no trends in the FUV light curves, and all fluctuations were consistent with statistical noise.

Finally, we examined the C IV line profile over time to see if we could identify radial velocity variations in the line over the orbital period. The orbital period of Swift J1753.5−0127 is unknown: a 3.24 hr photometric periodicity has been observed and was interpreted as a superhump modulation that occurs in low-mass ratio systems when a 3:1 orbital resonance is established within the accretion disk, which causes the disk to precess and exhibit a periodic emission modulation (Zurita et al. 2008; Haswell et al. 2001; Whitehurst 1988). Using an empirical relation between the orbital and superhump periods determined by Patterson et al. (2005), Zurita et al. found an orbital period range for Swift J1753.5−0127 between $3.18 < P_{\rm orb} < 3.24$ hr. We examined spectra extracted in time subintervals from 100 to 800 s. Unfortunately, the combination of low signal to noise in the individual spectra, the relatively low contrast between the line and continuum (the peak line flux is only 50% above the continuum flux), and the contamination of the line center by the interstellar absorption precluded obtaining reliable velocity shifts from C IV. The He II line was also too faint to yield significant results.

3.2. Interstellar Absorption and Reddening

There have been various estimates for the interstellar absorption and reddening along the line of sight to Swift J1753.5−0127. Fits to X-ray spectra in which hydrogen column density, $N_{\rm H}$, was allowed to vary have resulted in values of $N_{\rm H} = 1.7$–2.3×10^{21} cm^{-2} (Hiemstra et al. 2009; Miller et al. 2006; Morris et al. 2005). Cadolle Bel et al. (2007) and Durant et al. (2008) determined reddening values from the equivalent widths of the optical Na I D lines using the prescription of Munari & Zwitter (1997) and converted these to $N_{\rm H}$ after Bohlin et al. (1978). Using this method, Cadolle Bel et al. (2007) found $E(B-V) = 0.34 \pm 0.04$ and $N_{\rm H} = 2.0 \times 10^{21}$ cm^{-2}, while Durant et al. (2008) obtained $E(B-V) = 0.42 \pm 0.02$ and $N_{\rm H} = 2.45 \times 10^{21}$ cm^{-2}. Durant et al. speculated that the absorption internal to the system may vary over time, given the difference in their results from those of Cadolle Bel et al. Although there is some variation in determinations of $N_{\rm H}$, all of the derived values are comparable to the average total Galactic absorption along this line of sight (Morris et al. 2005; Durant et al. 2009).

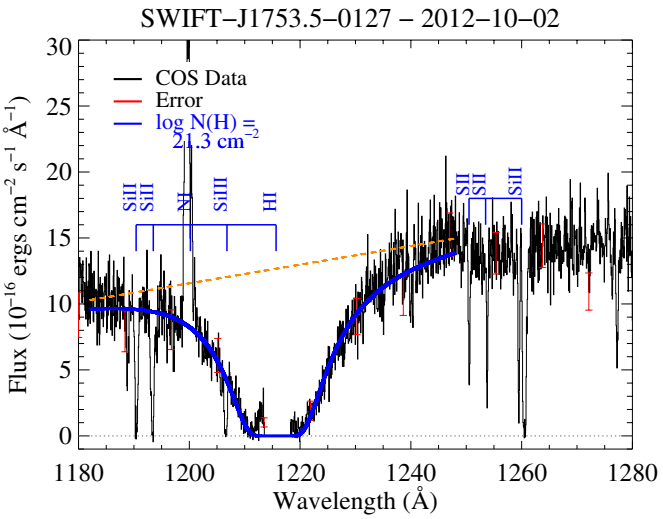

Figure 3. Lyα absorption line in the COS spectrum is fit to determine the hydrogen column density on the line of sight to Swift J1753.5−0127. Interstellar absorption and terrestrial airglow lines that were masked out in the fit are labeled in blue. The center of the Lyα profile is contaminated by airglow and is masked out. The solid blue line shows the model fit to the damping wings of the line profile, while the dashed yellow line shows the continuum normalization across the line.

(A color version of this figure is available in the online journal.)

We obtained values for both $E(B-V)$ and $N_{\rm H}$ from our UV spectra by fitting 2175 Å dust feature and the damping wings of the interstellar Lyα absorption line profile, respectively. To determine the reddening, we fit the 2175 Å feature in the NUV. Figure 2 shows the UV spectrum of Swift J1753.5−0127 in the region of the 2175 Å dust feature. The upper panel shows the observed spectrum normalized to a mean value of 1.0. Using the ccm_unred task from the IDL Astronomy User's Library[12], we dereddened the spectrum, stepping $E(B-V)$ from 0.00 to 1.00 in steps of 0.01 to find the reddening value that minimized the χ^2 deviation about a power-law fit to the residual. R_V was held fixed at 3.1. The best fit was $E(B-V) = 0.45$ with $\chi^2_\nu = 1.55$ (566 dof) for a 1400–3100 Å fit range. The reddening is consistent with the value found by Durant et al. (2008). Following the lead of Fitzpatrick (1999), who noted the large scatter about the mean in the amplitude of the 2175 Å feature in Galactic sight lines, we assume 20% uncertainty on our derived reddening and adopt $E(B-V) = 0.45 \pm 0.09$.

Figure 3 shows the Lyα absorption line and the best fit to the line profile. We fit the interstellar H I column density using a linear approximation of the observed (reddened) FUV continuum of Swift J1753.5−0127 and a Voigt profile for the Lyα resonance line. First, the geocoronal airglow emission (1213.5–1218.3 Å) was removed from the core of the interstellar absorption trough. A linear fit was then made across the Lyα region (1174–1270 Å), anchored on the blue end by the average continuum flux from 1175–1186 Å and on the red end by the average continuum flux from 1254–1258 Å. The Lyα absorber

[12] http://idlastro.gsfc.nasa.gov/homepage.html

is characterized by a column density, $N_{\rm H}$ (in units of $\rm cm^{-2}$), a Doppler-b parameter (in units of $\rm km\,s^{-1}$), and a velocity offset relative to the rest wavelength of the Lyα transition (in units of $\rm km\,s^{-1}$ relative to $\lambda_{\rm rest} = 1215.67$ Å). The velocity was fit by eye to produce a profile that evenly filled in the red and blue edges of the Lyα absorption trough ($v_{\rm Ly\alpha} = -10\,\rm km\,s^{-1}$). The b-value was chosen to be typical of the local interstellar medium ($10\,\rm km\,s^{-1}$; Redfield & Linsky 2004), although the b-value does not have a large influence on the heavily damped line profile observed for Swift J1753.5−0127. The interstellar column density was then varied until a best-fit value was found, with error bars defined as values of $N_{\rm H}$ that produce fits consistent with the 1σ photometric error bars in the line-core and wings. This procedure yielded $N_{\rm H} = 2.0 \pm 0.3 \times 10^{21}\,\rm cm^{-2}$.

If we use the reddening to infer $N_{\rm H}$ from the relation of Bohlin et al. (1978), we obtain a value larger than the one directly found from the Lyα line profile fitting, although they agree within the uncertainties on $N_{\rm H}$ and $E(B-V)$. Relating gas and dust absorption is subject to a number of uncertainties that could cause a slight discrepancy: we do not know the value of R_V for this sight line, and there is considerable scatter in the relationships between reddening and the size of 2175 Å feature (as noted above) and between gas and dust for individual sight lines (∼30% scatter about the Bohlin et al. relation). The gas along the line of sight to Swift J1753.5−0127 may also be more metal-rich than the average Galactic value, resulting in a larger reddening and a higher $N_{\rm H}$ found from the X-ray fitting compared to the fit to the Lyα line profile (whereas the Lyα interstellar line directly traces the neutral hydrogen along the line of sight, the $N_{\rm H}$ from the X-ray model fits includes absorption from helium and metals). Ultimately, the various methods for determining $N_{\rm H}$ and $E(B-V)$ for the sight line to Swift J1753.5−0127 have proven satisfactorily consistent within the uncertainties.

3.3. Accretion Disk Model Fits to the UV Spectrum

If we assume that the UV emission is dominated by the accretion disk, we can use disk model fits to the dereddened spectrum to determine black hole masses and accretion rates as a function of the distance to Swift J1753.5−0127. Most parameters are unknown or poorly constrained for this system, however, so our fits will be more instructive in placing limits on interesting values than in providing precise determinations. We fit the dereddened UV continuum with a grid of steady-state accretion disk model spectra constructed from summed, area-weighted blackbody spectra. The blackbody spectrum for each disk annulus was chosen to correspond to the theoretical, steady-state thin accretion disk temperature for that annulus. The models did not include disk irradiation.

Following Cheng et al. (1992), we can describe the observed flux density from a thin, steady-state, viscously heated accretion disk as:

$$f_\nu = f_0 \frac{\cos i}{d^2} (m\dot{m})^{2/3} \nu_{15}^{1/3} \int_{x_{\rm in}(\nu)}^{x_{\rm out}(\nu)} \frac{x^{5/3} dx}{e^x - 1}, \quad (1)$$

where $f_0 \simeq 2.9 \times 10^{-26}\,\rm erg\,cm^2\,s^{-1}\,Hz^{-1}$, d is the distance in kiloparsecs, i is the binary inclination, m ($=M_{\rm BH}/M_\odot$) is the mass of the black hole, $\dot{m}$ is the mass accretion rate in units of $10^{-9}\,M_\odot\,\rm yr^{-1}$, $\nu_{15} = \nu/10^{15}$ Hz, and $x = h\nu/kT(r)$ where $T(r)$ denotes the blackbody temperature (K) and radius (in units of 10^{11} cm) of each annulus.

The disk temperature at each annulus is a function of $M_{\rm BH}$, $\dot{m}$, and the radius. The overall temperature distribution in the disk depends on the inner and outer disk radii adopted. For the inner disk radius, $r_{\rm in}$, we examined models between two extreme values: $r_{\rm in} = 1.23\,r_g$ and $500\,r_g$, where r_g is the gravitational radius for a given black hole mass. The values represent differing predictions of the inner radius of the thin disk as extending to the ISCO for a maximally rotating Kerr black hole or truncated at larger radii under the ADAF model paradigm (Reynolds et al. 2010; Zhang et al. 2010). We set the outer disk radius, $r_{\rm out}$, to 60% of the Roche lobe radius. Following Zurita et al., we fixed $P_{\rm orb} = 3.23$ hr and the donor star mass to $M_2 = 0.3\,M_\odot$, which we used in conjunction with the black hole mass to set the binary geometry and $r_{\rm out}$.[13] Because the UV flux is dominated by emission from the inner disk annuli, the exact value of the $r_{\rm out}$ does not affect our fit results.

For these model parameters, the accretion disk model spectra for Swift J1753.5−0127 follow a $\nu^{1/3}$ power-law profile in the FUV spectral region. Therefore, we can use the normalization of the disk models to the observed FUV flux to constrain the black hole mass as a function of accretion rate, distance, and inclination. For the continuum region centered on 1470 Å (1425–1520 Å; $\nu = 2.04 \times 10^{15}$), we measure an average flux density of $f_\lambda = 6.48 \times 10^{-14}\,\rm erg\,cm^2\,s^{-1}\,Å^{-1}$. Converting to the frequency domain and substituting into Equation (6) of Cheng et al., we can express the mass of the black hole in Swift J1753.5−0127 as:

$$\frac{M_{\rm BH}}{M_\odot} = 0.546[\cos i]^{-3/2} \left[\frac{d}{1\ \rm kpc}\right]^3 \left[\frac{\dot{m}}{10^{-9}\ M_\odot\ \rm yr^{-1}}\right]^{-1}. \quad (2)$$

The binary inclination, distance, and mass accretion rate for Swift J1753.5−0127 are not known. The system does not show eclipses, which restricts inclinations to $i \lesssim 80°$. Reis et al. (2009) found $i = 55^{\circ +2}_{-7}$ based on model fits to X-ray reflection features. We adopt this as our default inclination but also examine how varying the inclination affects the other model parameters. (Note that the reflection fits assume that the disk extended to the ISCO at the time of the observations, which may not have been the case; see Section 4.)

Swift J1753.5−0127 has remained in the low/hard state throughout its outburst. Maccarone (2003) found that XRBs transition from the soft to the hard state between 1%–4% of the Eddington luminosity. The transition from hard state to soft can occur over a somewhat larger range of luminosities due to hysteresis effects (Maccarone & Coppi 2003). Here, we adopt an upper limit on the mass accretion rate of $\dot{m} \leqslant 0.05\dot{m}_{\rm Edd}$, where $\dot{m}_{\rm Edd} = L_{\rm Edd}/(0.1c^2)$, assuming a radiative efficiency of 10%. For the units in Equation (2), this corresponds to $\dot{m} \leqslant 1.097 \times m$. Since our data were taken at an X-ray luminosity several times smaller than the peak value (when the system remained in the low state), this upper limit is conservative.

Based on these parameter assumptions, we have generated upper limits on the distance to Swift J1753.5−0127 for given black hole masses based on fits to the dereddened UV continuum. These are given in Table 3. For the upper limits, we also assumed that the disk radius extends to the ISCO to maximize the potential disk emission. The distance could be higher for a lower inclination disk so we also present the upper limit on the distance for the extreme case of a face-on disk with $i = 0°$.

[13] Shaw et al. (2013) have claimed a 402 day modulation in the X-ray light curves of Swift J1753.5−0127. If this is attributed to a disk precession period, the inferred mass ratio for the system may be very low, $q \sim 0.002$, and M_2 may be much smaller than $0.3\,M_\odot$. This has a negligible effect on our models here, however, as the UV emission is only weakly dependent on the size of the outer accretion disk.

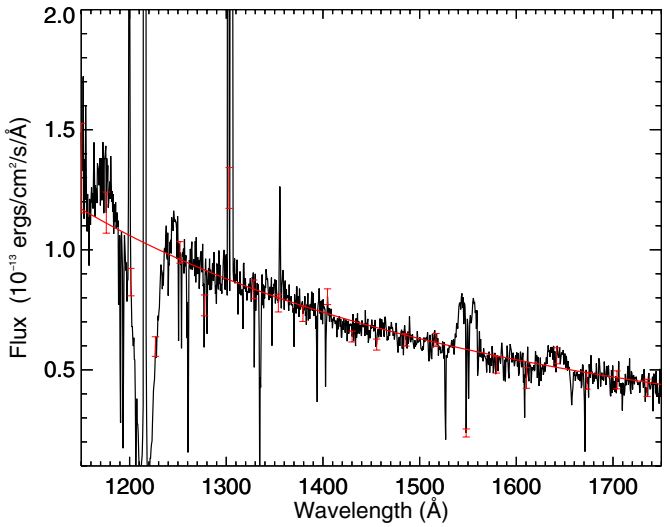

Figure 4. Dereddened spectrum of Swift J1753.5−0127 compared to a steady-state accretion disk model spectrum. The model has $M_{\rm BH} = 12.0\,M_\odot$, d = 5.1 kpc, and an inner disk radius of $r_{\rm in} = 1.23 r_g$. The inclination is $i = 55^\circ$. The spectrum has been binned to 0.5 Å spectral resolution. The model has not been formally fit to the spectrum but is overlaid by eye.

(A color version of this figure is available in the online journal.)

Table 3
Black Hole Mass and Distance Limits from UV Continuum Fits

$M_{\rm BH}$ ($M_\odot$)	$d(i = 55^\circ)$ (kpc)	$d(i = 0^\circ)$ (kpc)
3.0	⩽2.0	⩽2.6
5.0	⩽2.8	⩽3.7
7.0	⩽3.5	⩽4.6
9.0	⩽4.1	⩽5.5
12.0	⩽5.0	⩽6.6
15.0	⩽5.8	⩽7.7

Note. For $i = 55^\circ$ and $\dot{m} \leqslant 0.05 \dot{m}_{\rm Edd}$, Equation (2) reduces to $d \leqslant 0.955 m^{2/3}$. For $i = 0^\circ$, $d \leqslant 1.262 m^{2/3}$.

Figure 4 shows the $12\,M_\odot$ disk model compared to the data. The accretion disk models with viscous heating and no irradiation provide qualitatively good fits to the shape of the FUV continuum. The observed spectrum may be somewhat more blue than the model at the shortest FUV wavelengths, but we do not make a quantitative conclusion on this point because a small error in the adopted dereddening and/or the presence of unidentified emission features (such as C III 1175 Å and N V 1238, 1242 Å) could bias the continuum shape in this region. We are unable to distinguish between an accretion disk extending to the ISCO or one truncated at larger radii from the UV data alone (although see Section 4 for comparisons with the broadband SED). In either scenario, the UV is on the $\nu^{1/3}$ power-law portion of the disk SED, with peak emission occurring in the EUV for the truncated disk or in soft X-rays for the ISCO disk. The two radii give different results when fit to the data, however, since the ISCO model generates more UV flux; for example, for a 9 $M_\odot$ black hole at a 6 kpc distance, the inferred mass accretion rate must be 25% higher for the truncated disk compared to the ISCO radius to match the observed UV flux.

3.4. The Spectral Energy Distribution

In Figure 5, we plot the broadband SED for Swift J1753.5−0127 at the time of our observations. Table 4 gives

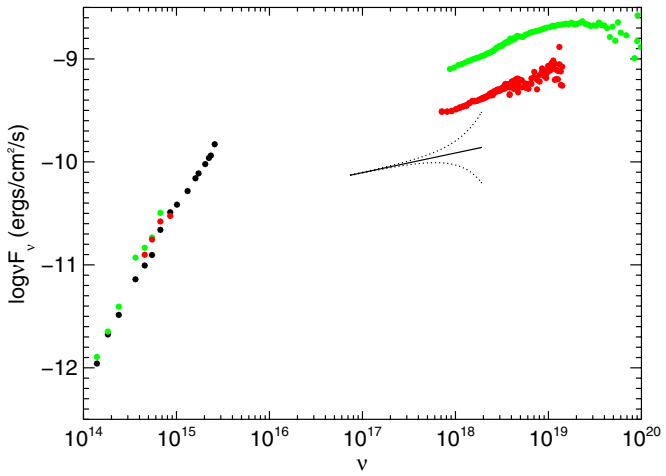

Figure 5. Broadband spectral energy distribution for the 2012 observations of Swift J1753.5−0127 is shown in black. The NIR, optical, and UV data have been dereddened assuming $E(B-V) = 0.45$. The X-ray data show the power-law fit to the *Swift* XRT observations with $N_{\rm H}$ fixed at 2.0×10^{21} cm^{-2}. The dashed lines show the uncertainties on the X-ray data. Shown in green and red, respectively, are the data from Cadolle Bel et al. (2007) and Durant et al. (2009).

(A color version of this figure is available in the online journal.)

Table 4
Spectral Energy Distribution

Band	Instrument	$\log(\nu)$ (Hz)	$\log(\nu F_\nu)$ (erg cm^{-2} s^{-1})
X-ray	*Swift*	16.87–18.29	−10.13–9.86[a]
FUV	COS	15.41	−9.83
FUV	COS	15.37	−9.94
FUV	COS	15.35	−9.96
FUV	COS	15.31	−10.02
FUV	COS	15.24	−10.11
FUV	COS	15.20	−10.16
NUV	COS	15.12	−10.28
NUV	COS	15.01	−10.42
U	UVOT	14.93	−10.49
B	SPIcam	14.83	−10.66
V	SPIcam	14.74	−10.90
R	SPIcam	14.66	−11.01
I	SPIcam	14.56	−11.14
J	NIC-FPS	14.38	−11.49
H	NIC-FPS	14.26	−11.68
K	NIC-FPS	14.14	−11.96

Notes. The optical-NIR data have been dereddened assuming $E(B-V) = 0.45$. The X-ray data have been corrected for interstellar absorption assuming $N_{\rm H} = 2.1 \times 10^{21}$ cm^{-2}.

[a] The X-ray data plotted is the model power-law component of a powerlaw * phabs fit in xspec.

the data we used for the SED for future reference. The NIR/optical/UV data were dereddened assuming $E(B-V) = 0.45$. For the X-ray data, we plot the power-law component of the model fit to the data and its uncertainties. In the figure, we also plot previous SEDs acquired in 2005 (three months after outburst start) and in 2007, with the optical/NIR points dereddened using our $E(B-V)$ value for a consistent comparison (Cadolle Bel et al. 2007; Durant et al. 2009).

A comparison of the X-ray SED from the three epochs shows that the X-ray fluxes have declined. The system has also faded in the optical/NIR. The NIR fluxes we observed are ≃90%, and the optical fluxes are ≃65% of those observed in 2005. The 2012 data are also fainter than the 2007 observations, with

fluxes that are ≃75% of the 2007 data in the optical. However, the shape of the optical/NIR SED has not changed significantly as it has faded: all three epochs show approximately power-law shapes, although a single power law cannot fit all of the optical/NIR data in any epoch. The new FUV observations show that the power-law shape extends at least to ≃1150 Å. The spectral break between the X-rays and lower energy data occurs at higher energies than the FUV.

4. DISCUSSION

4.1. The UV Spectrum

In this manuscript, we have presented the first UV spectrum of Swift J1753.5−0127, which is accompanied by contemporaneous X-ray, optical, and NIR observations. The dereddened UV spectrum is characterized by a continuum that smoothly increases to the blue and broad line emission from C IV, He II, and possibly N V. There are now high-quality FUV observations of three black hole XRBs in outburst: Swift J1753.5−0127, XTE J1118+480, and XTE J1859+226 (Haswell et al. 2002). The emission line spectra are different in each case. In XTE J1859+226, the UV spectrum has strong lines of C III, C IV, N V, O V, He II, and Si IV. That spectrum is richer in emission lines than Swift J1753.5−0127, and the N V line flux is nearly equal to that of C IV, whereas we do not confidently detect N V here. As noted by Haswell et al., the N V line can be suppressed relative to C IV by either photoionization by a harder X-ray ionizing spectrum or by relatively metal-poor abundances.

On the other hand, XTE J1118+480 shows the opposite effect: a much stronger N V emission and no C IV that has also been observed in A0620−00 (Froning et al. 2011) and is attributed to CNO processing in the accreted material. If Swift J1753.5−0127 had followed the evolutionary path proposed by Haswell et al. for XTE J1118+480 and A0620−00, wherein mass transfer was initiated after the donor star had already begun to move off the main sequence, their model would predict a current C/N abundance ratio for Swift J1753.5−0127 of $\log(C/N) \leqslant -2.3$, lower than in XTE J1118+480, where C IV is undetectable (Haswell et al. Figure 3; see also their discussion of why the low C V to N V ratio is unlikely to be caused by photoionization effects). Instead, the UV line spectrum of Swift J1753.5−0127 suggests little CNO processing, which is consistent with a system that initiated mass transfer at a shorter orbital period when the lower-mass donor star was still on the main sequence. More generally, the comparison of the three black hole XRB spectra in the UV shows that the complicated interplay of evolutionary history, metallicity, and photoionization leads to diverse spectroscopic signatures; observations of more systems will be valuable to constrain the physical processes underlying the line emission.

Swift J1753.5−0127 was stable during our observations to <10%, showing neither secular variability nor any evidence of the 3.24 hr orbital modulation seen in the optical light curves (Zurita et al. 2008), though the orbital modulation may have been below our detection threshold. Our longest continuous light curve in a single waveband was 5538 s, or about half of the 3.24 hr modulation. The Zurita et al. *R*-band light curves typically showed a 0.1 mag or smaller variation over those time scales, which is at the level of our sensitivity, assuming a similar amplitude in the FUV. Our NUV spectra show hints of variability on the ∼8% level but the 1400 s baseline in each spectrum is too short to determine if the orbital modulation is present. It is also unclear whether the modulation, believed to be due to superhumps, will still be present in Swift J1753.5−0127 several years after the initial outburst, although superhumps were seen in the light curve of XTE J1118+480 near quiescence (Zurita et al. 2002). The expected amplitude of the superhumps will likely be lower in the UV than in the optical, as the effect occurs in the cooler outer disk. Haswell et al. (2001) attributed superhumps in XRBs as an effect of changing disk area rather than changes in viscous dissipation in the disk, which might be more visible in the UV; however, this effect was in play for XRB disks dominated by irradiation, which may not be the case here (see below).

In Section 3.3, we fit the dereddened UV continuum spectrum with models of emission from a steady-state thin accretion disk. The models provide qualitatively acceptable fits to the spectral shape. The assumption that the UV emission is dominated by the thin disk is consistent with observations at other wavelengths and with system models. Reynolds et al. (2010) showed that a power law with a slope consistent with optically thin emission from a jet extended from the X-ray regime to longer wavelengths would have a negligible contribution to the optical/NIR flux. Their notional power-law component falls roughly an order of magnitude below our dereddened FUV fluxes. Similarly, an ADAF model fit to Swift J1753.5−0127 also predicts UV emission dominated by the thin disk (Zhang et al. 2010). Finally, Soleri et al. (2010) found that the jet is fainter in Swift J1753.5−0127 than in other hard state XRBs based on a comparison of its radio/X-ray flux ratio with the standard empirical relation. They too attribute the NIR/optical emission to the accretion disk.

Our disk models fit the UV continuum well given vicious dissipation in the disk as the only emission source. Disk models which include irradiation predict a flattening in the SED in the FUV that is inconsistent with our observed spectrum (see, e.g., Figures 7 and 9 of Chiang et al. 2010). This places Swift J1753.5−0127 in the category of "UV-hard" sources as defined by Hynes (2005), who compiled the UV/optical SEDs of several black hole XRBs in outburst and found that the systems either showed rising fluxes in the FUV (the UV-hard sources) or a peak in the NUV with a drop off in flux to shorter wavelengths (the "UV-soft") systems. The UV-hard sources were fit with viscously heated accretion disks while the UV-soft sources were dominated by emission from reprocessing of X-ray irradiation in the disk. (The UV-hard spectra can also be fit by irradiation models if the irradiating source is vertically extended above the disk plane, but the characteristic spectrum in that case remains different from the UV-soft profile; Hynes 2005; Dubus et al. 1999). One system, XTE J1859+226, has shown a transition during the outburst decline from being best fit with irradiation-dominated model spectra to models dominated by viscous heating (Hynes et al. 2002). The X-ray/optical cross-correlation function in Swift J1753.5−0127 also evolved from a clear signature of thermal reprocessing near outburst peak to an unusual profile at later times in which the optical and X-ray emission are anti-correlated, with the optical leading the X-rays (Hynes et al. 2009; Durant et al. 2008). A similar cross-correlation function was seen in XTE J1118+480, another XRB that remained in the low/hard state during its outburst (Kanbach et al. 2001). These correlations indicate a link between optical and X-ray emission, but not one that is explained by simple reprocessing of X-rays in the outer accretion disk.

Because the system parameters for Swift J1753.5−0127 are not well constrained, we could not use our disk model fits to directly determine the mass accretion rate in the disk. However,

by setting upper limits on the accretion rate as a fraction of the Eddington luminosity based on the fact that the system did not transition from the hard state to the soft state during the outburst, we were able to place limits on the mass of the black hole and the distance to the system based on the dereddened FUV continuum fluxes. We presented upper limits on the distance to Swift J1753.5−0127 for a range of black hole masses. These values are consistent with those found by Cadolle Bel et al. (2007, note that they present the minimum black hole mass for a given distance while we give the maximum distance for a given mass).

We are in closest agreement with the X-ray predictions for our models in which the disk is face-on rather than inclined. The Cadolle Bel et al. observations were conducted near outburst peak while ours were taken during the ongoing state in which Swift J1753.5−0127 has declined from its peak level but has not returned to quiescence. Accordingly, we expect that the disk accretion rate is lower now than in 2005, which is why our low inclination models (which produce more observable UV flux) are in closer agreement with the earlier black hole mass-distance relation. For a higher inclination, our more recent observations place tighter limits on the distance for a given black hole mass. Our limits are also conservative, since the mass accretion rate should be well below the 5% of Eddington transition luminosity seven years after the initial outburst. The hysteresis effect that can boost the transition luminosity for the hard to soft transition relative to the soft to hard one is a phenomenon of early outburst and will be seen near the peak rather than during the outburst decline (Maccarone & Coppi 2003). Moreover, Soleri et al. (2013) found that the X-ray spectrum of Swift J1753.5−0127 began to soften, but did not fully transition to the soft state, at an X-ray flux that was ≃5 times larger than our observed fluxes.

Although we cannot directly determine the black hole mass from our observations, our black hole mass/distance limits can be compared to current estimates of the distance to Swift J1753.5−0127, which lie roughly in the $d = 1$–10 kpc range. Zurita et al. (2008) used the non-detection of Swift J1753.5−0127 in optical catalogs prior to outburst to set the quiescent magnitude $V_{\rm quies} > 21$ and a distance $d > 1$ kpc for a M2 main sequence donor star. Their comparison of the outburst luminosities to various empirical relations for XRBs gave a distance range of ≃2.5–8 kpc. The interstellar hydrogen absorption column density in the spectrum, $N_{\rm H}$, of Swift J1753.5−0127 is comparable to the total Galactic column density in this direction, also suggesting a distance of d ∼6–7 kpc (Morris et al. 2005; Cadolle Bel et al. 2007; Durant et al. 2009). A 6 kpc distance would correspond to a black hole mass of $\geqslant 10.4\,M_{\odot}$.

We compared our disk model results to the system parameters adopted by Zurita et al. (2008): $M_{\rm BH} = 12.0\,M_{\odot}$ and $d = 5.5$ kpc. If we adopt those values, we must set $\dot{m} \simeq 2 \times 10^{-8}\,M_{\odot}\,{\rm yr}^{-1}$, or $0.08\,\dot{m}_{\rm Edd}$, to match the UV flux (for an $i = 55^{\circ}$ disk). Some of the ADAF models of XRBs have predicted that the accretion rate could be as high as $\dot{m} = 0.08$–$0.1\,\dot{m}_{\rm Edd}$ in the hard state (Esin et al. 1997; Zhang et al. 2010). If the accretion rate is <8% Eddington, the Zurita et al. parameters would require an adjustment to a higher black hole mass or a lower distance to be consistent with the UV fluxes. Once Swift J1753.5−0127 has returned to quiescence, there may be opportunities to place better constraints on the dynamical parameters of the binary system if the donor star can be observed. In that event, it will be of interest to revisit disk model fits to the UV spectrum to place tighter limits on the mass accretion rate through the thin disk during the outburst.

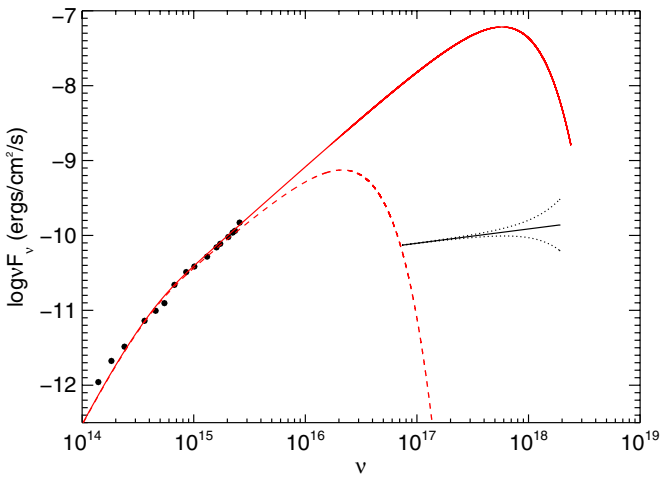

Figure 6. Steady-state accretion disk models are compared to the observed SED of Swift J1753.5−0127. The solid red line shows the 12.0 $M_{\odot}$ model shown in Figure 4 extended over the broadband SED. The dashed red line shows a model with the same parameters, except that the inner disk radius has been truncated at $r_{\rm in} = 100 r_g$.

(A color version of this figure is available in the online journal.)

4.2. The Broadband SED

Swift J1753.5−0127 has faded at all wavelengths since 2007, when previous broadband data were acquired (Durant et al. 2009; Soleri et al. 2010). The X-ray spectrum has dropped in luminosity by ≃60%. The optical/NIR data continue the slow decline seen since the 2005 outburst (Shaw et al. 2013). The shape of the SED has not changed dramatically, although the flux decline has been larger in the optical than in the NIR. The thin disk component fit to the UV also fits the optical fluxes reasonably well. There is a slight excess in the NIR compared to the model. Some of the excess NIR flux can be recovered by increasing the outer disk radius above the $0.6 R_{L_1}$ value we used, but even disks extending to 90% of the Roche lobe radius don't recover all of the NIR emission. The excess may indicate an additional contribution from either the jet, the hot flow component of an ADAF, or synchrotron emission by non-thermal electrons in the hot corona (Zhang et al. 2010; Veledina et al. 2013).

As noted in Section 3.3, we could not distinguish between accretion disks whose inner radii extend to the ISCO versus those that are truncated at a larger radius from the UV data alone. However, if we compare the disk models to the broadband SED, we find a discrepancy between the observed UV and X-ray fluxes if the accretion disk extends to the ISCO. This is illustrated in Figure 6, where we plot our 12 $M_{\odot}$ model on the SED. The model that fits the UV fluxes well exceeds the X-ray component by two orders of magnitude.

There are two ways to resolve this discrepancy. First, if the UV is not dominated by the steady-state thin disk, a disk that extends to the ISCO can be present. The models of Miller et al. (2006) and Reynolds et al. (2010), for example, include a thermal component from a thin disk extending to the ISCO. Their disk components (assuming a 10 $M_{\odot}$ black hole and 8.5 kpc distance) will not match the UV: they fall a factor of five below our 2011 observed fluxes, which moreover will be fainter than the 2006/2007 data fit by these groups. In this event, the NIR/optical/UV data would need a substantial contribution from an additional component with a power-law shape. In some XRBs, the UV emission is dominated by a single temperature blackbody component with a small emitting area, attributed either to the

hotspot where the in falling accretion stream impacts the outer disk or to emission at the transition radius between the thin disk and the ADAF (Froning et al. 2011; McClintock et al. 1995; Hynes & Robinson 2012). These systems were in quiescence, however, not the active state observed in Swift J1753.5−0127, and a single temperature blackbody does not fit the slope of the UV data. Given that Swift J1753.5−0127 is in outburst, has a UV SED consistent with steady-state accretion disk models, and, as discussed above, other emission components (such as the jet or the X-ray hot flow) are unlikely to contribute substantially at these wavelengths, we believe that the UV emission is dominated by the thin disk.

Second, the disk could be truncated at a larger radius than the ISCO. In Figure 6, we show that a disk model whose inner radius is truncated at $r_{\rm in} = 100 r_g$ fits the optical/UV data without exceeding the X-ray flux. The inner radius is larger than the $r_{\rm in} = 10 - 50 r_g$ radii cited by Reynolds et al. (2010) but not as large as the $250 r_s$ ($500 r_g$) radius adopted by Zhang et al. (2010) for their ADAF model fits. The low luminosity in the X-ray band relative to the UV underscores the importance of understanding the energy balance in the low state of XRBs near the black hole: significant mass loss from the system and/or enormous energy loss via advection is required to reconcile the observational discrepancy.

Chiang et al. (2010) also noted that the X-ray data in Swift J1753.5−0127 are under-luminous relative to optical/UV fluxes, with accretion disk model fits to the X-rays under predicting the longer wavelength data. The deviation between the extrapolated X-ray model fits and the optical/UV data increased with time further from outburst peak. They were able to fit the SED with a truncated, irradiated disk to fit the optical/UV and invoked a separate soft component to fit the X-rays. They did not favor that model because the irradiated area of the disk was implausibly small and instead attributed the optical/UV data to synchrotron radiation from the jet. As we noted above, however, the FUV data are inconsistent with the irradiated disk models. Given that the jet in Swift J1753.5−0127 is under-luminous compared to other hard state XRBs, and the radio to optical spectral indices are inconsistent with the compact steady jet extending to the NIR/optical waveband, the evidence argues against jet-dominated emission in the optical/UV (Soleri et al. 2010).

5. CONCLUSIONS

We obtained the first ultraviolet spectra of the black hole XRB, Swift J1753.5−0127, using the COS on the *HST*. The dereddened UV spectrum has a blue continuum and broad (FHWM $\simeq 3500\,{\rm km\,s^{-1}}$) emission lines of C IV, He II, and possibly N V. The UV count rate was stable to <10% during the observations. We fit the 2175 Å interstellar feature to determine an estimate of the interstellar reddening, $E(B-V) = 0.45 \pm 0.09$. By fitting the interstellar Lyα line profile, we also derived the neutral hydrogen column density along the line of sight to Swift J1753.5−0127 as $N_{\rm H} = 2.0 \pm 0.3 \times 10^{21}\,{\rm cm^{-2}}$.

We fit models of a steady-state accretion disk to the dereddened UV continuum. A viscously heated disk with no reprocessing of X-ray irradiation included provided a good fit to the shape of the spectrum. The binary system parameters are not well constrained, but by assuming that the mass accretion rate of Swift J1753.5−0127 (which has never transitioned out of the low/hard state during the outburst) is below 5% of the Eddington rate, we placed limits on the distance for a range of black hole mass values. Based on estimates of the distance to the source, a black hole mass well above $3.0\,M_\odot$ is favored, although the lower-mass values are not fully ruled out.

We presented a broadband NIR/optical/UV/X-ray SED of Swift J1753.5−0127. The source has faded at all wavelengths since previous broadband observations in 2007, and the X-ray power-law spectral index has steepened. The UV component of the SED extends the power law seen in the optical to shorter wavelengths with no evidence of a spectral break. However, the thin disk component required to fit the UV fluxes will exceed the observed X-ray data unless some truncation of the inner disk beyond the ISCO is adopted and large mass loss from the system or energy loss via advection into the black hole takes place.

Thanks to M. Cadolle Bel and M. Durant for sharing their spectral energy distribution data. R.I.H. acknowledges support from the National Science Foundation under Grant No. AST-0908789. This work was based on observations made with the NASA/ESA *Hubble Space Telescope*, which is operated by the Association of Universities for Research in Astronomy, Inc., under NASA contract NAS 5-26555. These observations are associated with program 12039. This work was supported by NASA grant NNX08AC146 to the University of Colorado at Boulder. Some of the data presented in this paper were obtained from the Multimission Archive at the Space Telescope Science Institute (MAST). Support for MAST for non-*HST* data is provided by the NASA Office of Space Science via grant NNX09AF08G and by other grants and contracts.

Facilities: HST (COS), *Swift*, ARC

REFERENCES

Armas Padilla, M., Degenaar, N., Russell, D. M., & Wijnands, R. 2013, MNRAS, 428, 3083
Arnaud, K. A. 1996, in ASP Conf. Ser. 101, Astronomical Data Analysis Software and Systems V, ed. G. Jacoby & J. Barnes (San Francisco, CA: ASP), 17
Bayless, A. J., Robinson, E. L., Hynes, R. I., Ashcraft, T. A., & Cornell, M. E. 2010, ApJ, 709, 251
Bohlin, R. C., Savage, B. D., & Drake, J. F. 1978, ApJ, 224, 132
Brocksopp, C., Bandyopadhyay, R. M., & Fender, R. P. 2004, NewA, 9, 249
Burrows, D. N., Hill, J. E., Nousek, J. A., et al. 2005, SSRv, 120, 165
Cadolle Bel, M., Ribó, M., Rodriguez, J., et al. 2007, ApJ, 659, 549
Cadolle Bel, M., Rodriguez, J., Goldwurm, A., et al. 2005, ATel, 574, 1
Cheng, F. H., Horne, K., Panagia, N., et al. 1992, ApJ, 397, 664
Chiang, C. Y., Done, C., Still, M., & Godet, O. 2010, MNRAS, 403, 1102
Danforth, C. W., Keeney, B. A., Stocke, J. T., Shull, J. M., & Yao, Y. 2010, ApJ, 720, 976
Dubus, G., Lasota, J.-P., Hameury, J.-M., & Charles, P. 1999, MNRAS, 303, 139
Durant, M., Gandhi, P., Shahbaz, T., Peralta, H. H., & Dhillon, V. S. 2009, MNRAS, 392, 309
Durant, M., Gandhi, P., Shahbaz, T., et al. 2008, ApJL, 682, L45
Esin, A. A., McClintock, J. E., & Narayan, R. 1997, ApJ, 489, 865
Fender, R. 2006, in Compact Stellar X-ray Sources, ed. W. Lewin & M. van der Klis (Cambridge: Cambridge Univ. Press), 381
Fender, R., Corbel, S., Tzioumis, T., et al. 1999, ApJL, 519, L165
Fender, R., Garrington, S., & Muxlow, T. 2005, ATel, 558, 1
Fitzpatrick, E. L. 1999, PASP, 111, 63
Froning, C. S., Cantrell, A. G., Maccarone, T. J., et al. 2011, ApJ, 743, 26
Green, J. C., Froning, C. S., Osterman, S., et al. 2012, ApJ, 744, 60
Haardt, F., & Maraschi, L. 1991, ApJL, 380, L51
Halpern, J. P. 2005, ATel, 549, 1
Haswell, C. A., Hynes, R. I., King, A. R., & Schenker, K. 2002, MNRAS, 332, 928
Haswell, C. A., King, A. R., Murray, J. R., & Charles, P. A. 2001, MNRAS, 321, 475
Hearty, F. R., Morse, J., Beland, S., et al. 2004, Proc. SPIE, 5492, 1623
Hiemstra, B., Soleri, P., Méndez, M., et al. 2009, MNRAS, 394, 2080
Holland, S. T., et al. 2012, Cosmic Origins Spectrograph Instrument Handbook, Version 5.0 (Baltimore, MD: STScI)

Hunt, L. K., Mannucci, F., Testi, L., et al. 1998, AJ, 115, 2594
Hynes, R. I. 2005, ApJ, 623, 1026
Hynes, R. I., Brien, K. O., Mullally, F., & Ashcraft, T. 2009, MNRAS, 399, 281
Hynes, R. I., Haswell, C. A., Chaty, S., Shrader, C. R., & Cui, W. 2002, MNRAS, 331, 169
Hynes, R. I., Mauche, C. W., Haswell, C. A., et al. 2000, ApJL, 539, L37
Hynes, R. I., & Robinson, E. L. 2012, ApJ, 749, 3
Jain, R. K., Bailyn, C. D., Orosz, J. A., McClintock, J. E., & Remillard, R. A. 2001, ApJL, 554, L181
Kanbach, G., Straubmeier, C., Spruit, H. C., & Belloni, T. 2001, Natur, 414, 180
Kriss, G. A. 1994, in ASP Conf. Ser. 61, Astronomical Data Analysis Software & Systems III, ed. D. R. Crabtree, R. J. Hanisch, & J. Barnes (San Francisco, CA: ASP), 437
Maccarone, T. J. 2003, A&A, 409, 697
Maccarone, T. J., & Coppi, P. S. 2003, MNRAS, 338, 189
Markoff, S., Falcke, H., & Fender, R. 2001, A&A, 372, L25
McClintock, J. E., Horne, K., & Remillard, R. A. 1995, ApJ, 442, 358
McClintock, J. E., & Remillard, R. A. 2000, ApJ, 531, 956
McClintock, J. E., & Remillard, R. A. 2006, in Compact Stellar X-ray Sources, ed. W. Lewin & M. van der Klis (Cambridge: Cambridge Univ. Press), 157
Merloni, A., & Fabian, A. C. 2001a, MNRAS, 328, 958
Merloni, A., & Fabian, A. C. 2001b, MNRAS, 321, 549
Miller, J. M., Homan, J., & Miniutti, G. 2006, ApJL, 652, L113
Morris, D. C., Burrows, D. N., Racusin, J., et al. 2005, ATel, 552, 1
Morton, D. C. 1978, ApJ, 222, 863
Mostafa, R., Mendez, M., Hiemstra, B., et al. 2013, MNRAS, 431, 2341
Munari, U., & Zwitter, T. 1997, A&A, 318, 269
Narayan, R., Barret, D., & McClintock, J. E. 1997, ApJ, 482, 448
Narayan, R., & Yi, I. 1995, ApJ, 444, 231
Osterman, S., Green, J., Froning, C., et al. 2011, Ap&SS, 335, 257
Palmer, D. M., Barthelmey, S. D., Cummings, J. R., et al. 2005, ATel, 546, 1
Patterson, J., Kemp, J., Harvey, D. A., et al. 2005, PASP, 117, 1204
Ramadevi, M. C., & Seetha, S. 2007, MNRAS, 378, 182
Redfield, S., & Linsky, J. L. 2004, ApJ, 613, 1004
Reis, R. C., Fabian, A. C., Ross, R. R., & Miller, J. M. 2009, MNRAS, 395, 1257
Reynolds, M. T., Miller, J. M., Homan, J., & Miniutti, G. 2010, ApJ, 709, 358
Roming, P. W. A., Kennedy, T. E., Mason, K. O., et al. 2005, SSRv, 120, 95
Russell, D. M., Fender, R. P., Hynes, R. I., et al. 2006, MNRAS, 371, 1334
Shakura, N. I., & Sunyaev, R. A. 1973, A&A, 24, 337
Shapiro, S. L., Lightman, A. P., & Eardley, D. M. 1976, ApJ, 204, 187
Shaw, A. W., Charles, P. A., Bird, A. J., et al. 2013, MNRAS, 433, 740
Soleri, P., Fender, R., Tudose, V., et al. 2010, MNRAS, 406, 1471
Soleri, P., Muñoz-Darias, T., Motta, S., et al. 2013, MNRAS, 429, 1244
Still, M., Roming, P., Brocksopp, C., & Markwardt, C. B. 2005, ATel, 553, 1
Sunyaev, R. A., & Truemper, J. 1979, Natur, 279, 506
Tananbaum, H., Gursky, H., Kellogg, E., Giacconi, R., & Jones, C. 1972, ApJL, 177, L5
Thorne, K. S., & Price, R. H. 1975, ApJL, 195, L101
Torres, M. A. P., Steeghs, D., Blake, C., et al. 2005, ATel, 566, 1
Veledina, A., Poutanen, J., & Vurm, I. 2013, MNRAS, 430, 3196
Whitehurst, R. 1988, MNRAS, 232, 35
Zhang, H., Yuan, F., & Chaty, S. 2010, ApJ, 717, 929
Zurita, C., Casares, J., Shahbaz, T., et al. 2002, MNRAS, 333, 791
Zurita, C., Durant, M., Torres, M. A. P., et al. 2008, ApJ, 681, 1458